

LASER APPLICATIONS AND OTHER TOPICS IN QUANTUM ELECTRONICS https://doi.org/10.1070/QEL16730

Comparative analysis of waveguide plasmon–polariton refractometers based on excitation of surface, symmetric, and antisymmetric plasmon modes

A.V. Dyshlyuk, O.B. Vitrik, Yu.N. Kulchin

Abstract. **We present the results of a numerical study of three waveguide refractometer configurations based on surface plasmon resonance: a refractometer without a buffer layer based on exciting a surface plasmon mode, and refractometers with a buffer layer based on exciting symmetric and antisymmetric plasmon modes. It is found that the best metrological characteristics are inherent in the refractometer based on the symmetric plasmon mode: the cumulative advantage in spectral sensitivity and width of the resonance dip attains two orders of magnitude as compared to the refractometer based on antisymmetric plasmon mode and one order of magnitude as compared to the refractometer without a buffer layer. For measuring local variations of the refractive index in a thin layer the advantage of using the symmetric plasmon mode is less expressed and amounts to nearly 20 and 6 times, respectively. It is shown that higher metrological characteristics of the refractometer based on symmetric plasmon mode are achieved at the expense of its compactness: the length of the sensitive segment in such a refractometer may exceed that of the refractometers without the buffer layer and those based on the antisymmetric mode by three orders of magnitude. The minimal length of the sensitive segment is possible in the refractometer based on the antisymmetric plasmon mode, which, however, possesses the worst metrological characteristics. As to the fabrication simplicity, the scheme without the buffer layer seems most attractive. This scheme occupies the intermediate position between the refractometers based on symmetric and antisymmetric plasmon modes both in metrological parameters and in the length of the sensitive segment.**

Keywords: *surface plasmon resonance, waveguide plasmon–polariton refractometer, symmetric plasmon mode, antisymmetric plasmon mode, chemosensorics, biosensorics.*

1. Introduction

Refractometric sensors based on surface plasmon resonance (SPR) represent a promising line of the development in modern bio- and chemosensorics [1–6]. The sensors of this type exploit the resonance excitation of surface plasmon–polariton waves, i.e., coupled oscillations of electron density and electromagnetic field, arising at the interface between a metal and a dielectric, for high-accuracy measurement of the refractive index (RI) near the interface [5, 6]. The most widely used scheme of a SPR refractometer is the Krechman configuration, in which the surface plasmons are excited by a beam of light incident from inside a prism on its metallised face at the angle exceeding that of total internal reflection [5, 6]. Under the condition of phase matching between the exciting beam and the plasmon wave, the total internal reflection is frustrated, and the energy of the incident beam is transferred to surface plasmons. This leads to the formation of a resonance dip in the angular (or frequency) spectrum of the reflected light, the position of which strongly depends on the refractive index of the medium near the metallic film, which provides the possibility of refractometric measurements. For using such refractometer as a bio- or chemosensor, a layer of ligand molecules (the receptors that can react with a certain type of analyte molecules) is deposited on the surface of the metallic film [5, 6]. The association reaction between the ligand and the analyte leads to the local change in the refractive index near the metallic film, which can be detected by the shift of the resonance dip in the spectrum of the recorded signal.

The Krechman scheme is well approved and finds wide application in laboratory biochemical studies; however, it is inconvenient for designing compact, portable and cheap biosensor devices, including single-use ones, aimed for using under field conditions. Therefore, significant attention of researchers is attracted by waveguide SPR refractometers, in which plasmon–polariton waves are excited by the radiation propagating through dielectric waveguides [6–9]. The sensors of this type, in contrast to the Krechman configuration, provide miniaturisation and interfacing of sensor devices with the elements of fibre and integral optics, performing measurements in hardly accessible places, as well as cost reduction of plasmon–polariton bio- and chemosensor systems [6–9].

There are different schemes of designing plasmon–polariton refractometers. The simplest one is the configuration that represents a waveguide analogue of the Krechman scheme, in which the metallic film is deposited directly on the light-guiding core of the optical waveguide [6]. The schemes with an intermediate layer between the core and the metallic film are also known. In the latter case the SPR refractometer can operate using the excitation of both the symmetric plasmon mode (SPM), also referred to as long-range surface plasmon, and the antisymmetric plasmon mode (ASPM), also referred to as short-range surface plasmon, which arise as a result of hybridisation of plasmon waves, propagating on different sides of the thin metallic film [6].

A.V. Dyshlyuk Far Eastern Federal University, ul. Sukhanova 8, 690091 Vladivostok, Russia; Vladivostok State University of Economics and Service, ul. Gogolya 41, 690014 Vladivostok, Russia; e-mail: anton_dys@iacp.dvo.ru;
O.B. Vitrik, Yu.N. Kulchin Far Eastern Federal University, ul. Sukhanova 8, 690091 Vladivostok, Russia; Institute of Automation and Control Processes, Far Eastern Branch, Russian Academy of Sciences, ul. Radio 5, 690041 Vladivostok, Russia; e-mail: oleg_vitrik@mail.ru

Received 12 May 2018
Kvantovaya Elektronika **48** (9) 867–878 (2018)
Translated by V.L. Derbov

Note that in the SPR refractometer without a buffer layer, as in the Krechman scheme, the RI of the waveguide layer, as a rule, essentially exceeds that of the surrounding medium. For this reason, the propagation constants of the plasmon modes propagating on different sides of the metallic film strongly differ, and even if the thickness of the film is small, the hybridisation of these modes practically does not occur. In this case, the excited plasmon mode is localised at the interface between the metal and the external medium and has the characteristics close to those of a plasmon mode on the surface of bulk metal. Therefore, below we refer this mode to as surface plasmon mode.

The symmetric, antisymmetric, and surface plasmon modes essentially differ in propagation constants, damping, degree of field localisation, and sensitivity to the refractive index of the external medium [6]. In literature, there is no current opinion on the issue which mode is most suitable for using in a SPR refractometer. The authors proposing configurations of waveguide SPR refractometers based on SPM refer to their lower losses and, correspondingly, narrower resonance dip and higher spectral sensitivity [10–12]. In other papers the authors emphasise the better field localisation of the antisymmetric mode and its high losses, providing higher sensitivity to the local RI changes in a thin layer and minimal dimensions of the sensitive element [13–14]. In Ref. [6] the SPM, ASPM, and surface plasmon mode are thoroughly quantitatively compared from the point of view of their use in the Krechman SPR refractometer. However, as far as we know, for waveguide plasmon–polariton refractometers such comparison has not been performed yet.

The aim of the present paper is to analyse comparatively the waveguide plasmon–polariton refractometers based on the excitation of surface, symmetric and antisymmetric plasmon modes.

2. Object and methods of study

We studied three configurations of a waveguide SPR refractometer: a refractometer without a buffer layer (Fig. 1a) and refractometers having a buffer layer and using symmetric and antisymmetric plasmon modes (Fig. 1b). In all three cases, the refractometer is formed by three waveguide segments: 1 and 3 are input and output segments of the initial waveguide without a metallic film, and 2 is the sensitive metallised segment. The metallic film contacts a liquid external medium, whose refractive index n_{ext} is the quantity to be measured and is expected to lie within the limits from nearly 1.33 to 1.45. As a material for the metallic film, the silver was chosen, for which the data on the complex permittivity were taken from handbook [15]. To provide the possibility of exciting plasmon–polariton waves in the metallic film, the polarisation direction of the electric field of the guided radiation was chosen to lie in the plane of Fig. 1.

The waveguide layer parameters were chosen to provide its single-mode operation, so that the guided radiation in segments 1 and 3 is described by the only fundamental mode with the chosen polarisation.

To analyse the light propagation through segment 2, we use two different approaches. In the first case, the guided radiation is presented as a sum of two hybrid modes of the

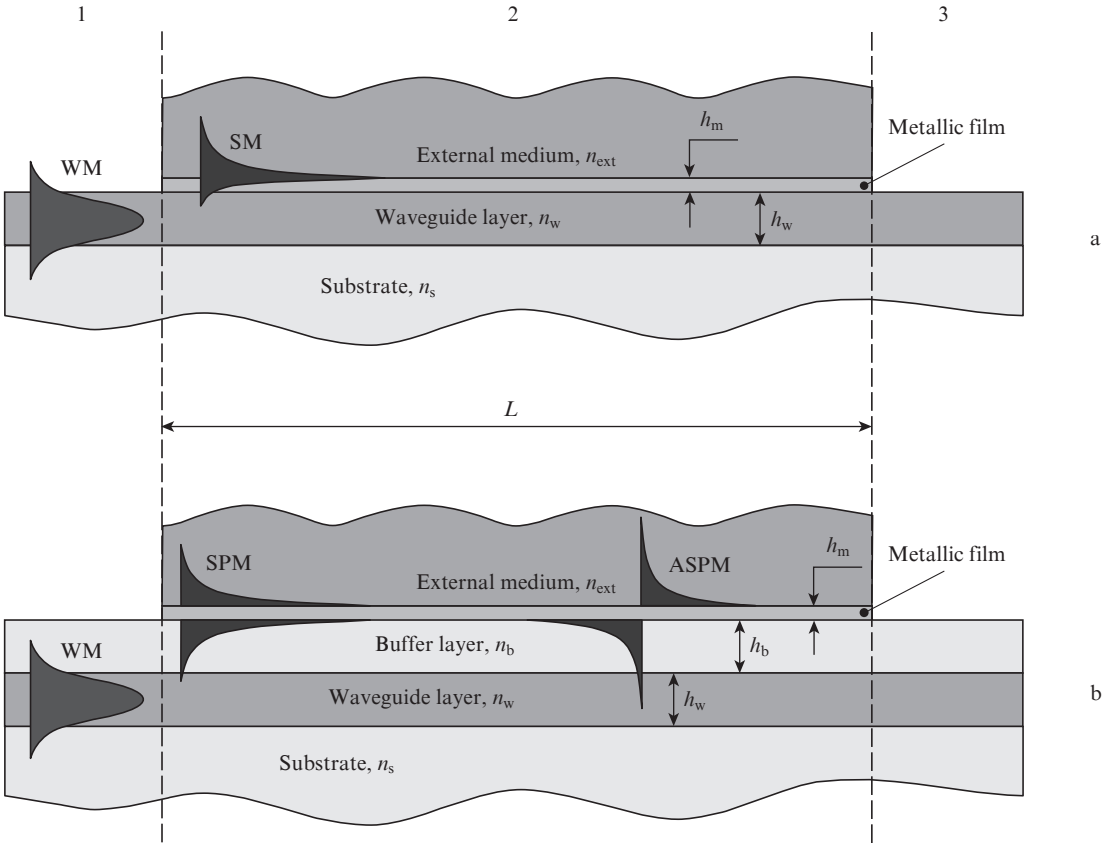

Figure 1. Schematic of the structures under study: (a) SPR refractometer without a buffer layer based on the excitation of the surface plasmon mode and (b) SPR refractometer with a buffer layer based on the excitation of symmetric and antisymmetric plasmon modes.

multilayer waveguide structure. In the second case, the guided radiation is composed of a simpler waveguide and plasmon modes, considered separately, and their interaction, arising when their propagation constants coincide or are close to each other, is described using the coupled mode theory and leads to a change in their amplitudes in the process of propagation [16]. The first approach is more convenient for computations and we use it for numerical simulations, while the second approach is physically clearer, and we use it for preliminary analysis and interpretation of numerical results.

The numerical simulation was performed using the commercial software package Lumerical Mode Solutions™, by means of which we calculated the mode profiles and propagation constants for each of the three segments, including the hybrid modes of segment 2, the amplitudes of modes, excited at the interfaces between the segments, the distribution of the total field of the guided radiation in segment 2, and the transmission coefficient of the entire structure as a power ratio of fundamental modes in segments 3 and 1. To simplify the calculations we considered the problem in 2D geometry, corresponding to an ideal planar optical waveguide. However, the obtained results can be easily generalised over the case of similar integrated optical waveguide structure with a rectangular cross section, and also provide qualitative representation of the metrological characteristics of analogous fibre-optical plasmon–polariton refractometers.

In all cases the materials and the geometric parameters of the waveguide structure were chosen to provide phase matching at a certain resonance wavelength λ_{SPR} between the waveguide and plasmon modes, considered separately. The coupling of modes leads to the losses of the guided radiation at $\lambda = \lambda_{SPR}$ due to the transfer of its energy to the plasmon mode and, thus, to the formation of a dip at the resonance wavelength in the transmission spectrum of the entire structure. The change in the external medium RI affects the propagation constant of the plasmon mode, which leads to the shift of the resonance dip and, therefore, provides the possibility of refractometric measurements.

The main metrological characteristic of a SPR refractometer is its spectral sensitivity [6]

$$S_{RI} = \frac{d\lambda_{SPR}}{dn_{ext}} = \frac{d\lambda_{SPR}}{dn'_{SP}} \frac{dn'_{SP}}{dn_{ext}} = S_1 S_2,$$

where n'_{SP} is the real part of the effective refractive index (ERI) of the plasmon mode; $S_1 = d\lambda_{SPR}/dn'_{SP} = [(dn_{wg}/d\lambda) - (dn'_{SP}/d\lambda)]^{-1}$ is the instrumental sensitivity determined by the intersection angle of dispersion curves of the waveguide and the plasmon mode; λ is the wavelength; n_{wg} is the ERI of the waveguide mode; and $S_2 = dn'_{SP}/dn_{ext}$ is the physical sensitivity of the plasmon mode ERI to the refractive index of external medium.

Besides the sensitivity, the resolution of refractometric measurements also depends on the width and depth of the resonance dip, the level of measurements system noises and other factors. However, for comparison of different schemes of SPR refractometers, it is sufficient to keep in mind that the resolution σ is inversely proportional to the spectral sensitivity and the dip contrast, defined as the ratio of its depth to its width [6].

Since in waveguide SPR refractometers the attenuation at the resonance wavelength can reach a few orders of magnitude and it is convenient to present the transmission spectra in the logarithmic scale, it seems rational to use the full width at square root minimum (FWSRM), corresponding to the half-width of the dip in the logarithmic scale, rather than the traditional half-width. As shown by calculations, this logarithmic half-width increases with increasing plasmon mode losses near λ_{SPR} and with decreasing crossing angle of its dispersion curve with the appropriate curve of the waveguide mode.

The depth of the resonance dip is determined, first, by the length of the sensitive segment L. The best resolution is provided at the maximal depth of the dip; however, if the latter exceeds the dynamic range of the used spectrum analyser, the shape of the recorded dip may be distorted due to the noise effect. With this fact taken into account, the length of the sensitive segment in all studied configurations was chosen such that the maximal attenuation at the resonance wavelength amounted to ~ 80 dB, which approximately corresponds to the dynamic range of up-to-date optical spectrum analysers (e.g., Yokogawa AQ6370D).

Thus, for comparison of different configurations of the SPR refractometer we will use the figure of merit (FOM) defined as a ratio of the spectral sensitivity to the logarithmic half-width of the resonance dip. The resolution of the refractometric measurements is inversely proportional to FOM, so that its maximal value corresponds to the best SPR refractometer configuration.

For bio- and chemosensor applications, the depth of penetration of the excited plasmon mode into the external medium (d_{SP}), determined at the 1/e level of the maximal intensity, is also an important characteristic. This is because the sensitive layer of ligand molecules may have the thickness (d_{lig}) much smaller than the above penetration depth. In this case, as shown in Ref. [6], it is reasonable to use the notion of local sensitivity $S_{loc} \propto S_{RI}(d_{lig}/d_{SP})$, which characterises the sensitivity of the plasmon mode ERI to the refractive index variations in a thin layer near the metallic film.

Keeping in mind the above considerations, we assume that the resolution of the refractometric measurements in a thin sensitive layer is proportional to the so-called local resolution coefficient (LRC), which we define as a ratio of the penetration depth d_{SP} and FOM. The RLC will be used for comparison of the local resolution of different configurations of SPR refractometers (the minimal value of RLC corresponds to the best configuration).

3. Results of the study

3.1. SPR refractometer without a buffer layer

From the practical point of view, it is reasonable to use the most widespread materials for constructing a waveguide SPR refractometer, so we choose SiO_2 ($n_s \approx 1.45$ [15]) as a substrate material and PMMA ($n_w \approx 1.49$ [17]) as a waveguide layer material. In this case, as shown by numerical calculations, for the waveguide layer thickness $h_w = 1.5$ μm and the refractive index of the external medium $n_{ext} = 1.4$ the dispersion curves of the surface plasmon mode and the waveguide mode (WM) considered separately intersect in the near infrared range (Fig. 2a, dotted curves). By the surface plasmon mode considered separately, we mean the mode of the metallic film, localised near the boundary between the metal and the external medium. The metal film contacts the half-infinite external medium on one side and the half-infinite dielectric having the refractive index n_w on the other side. By the wave-

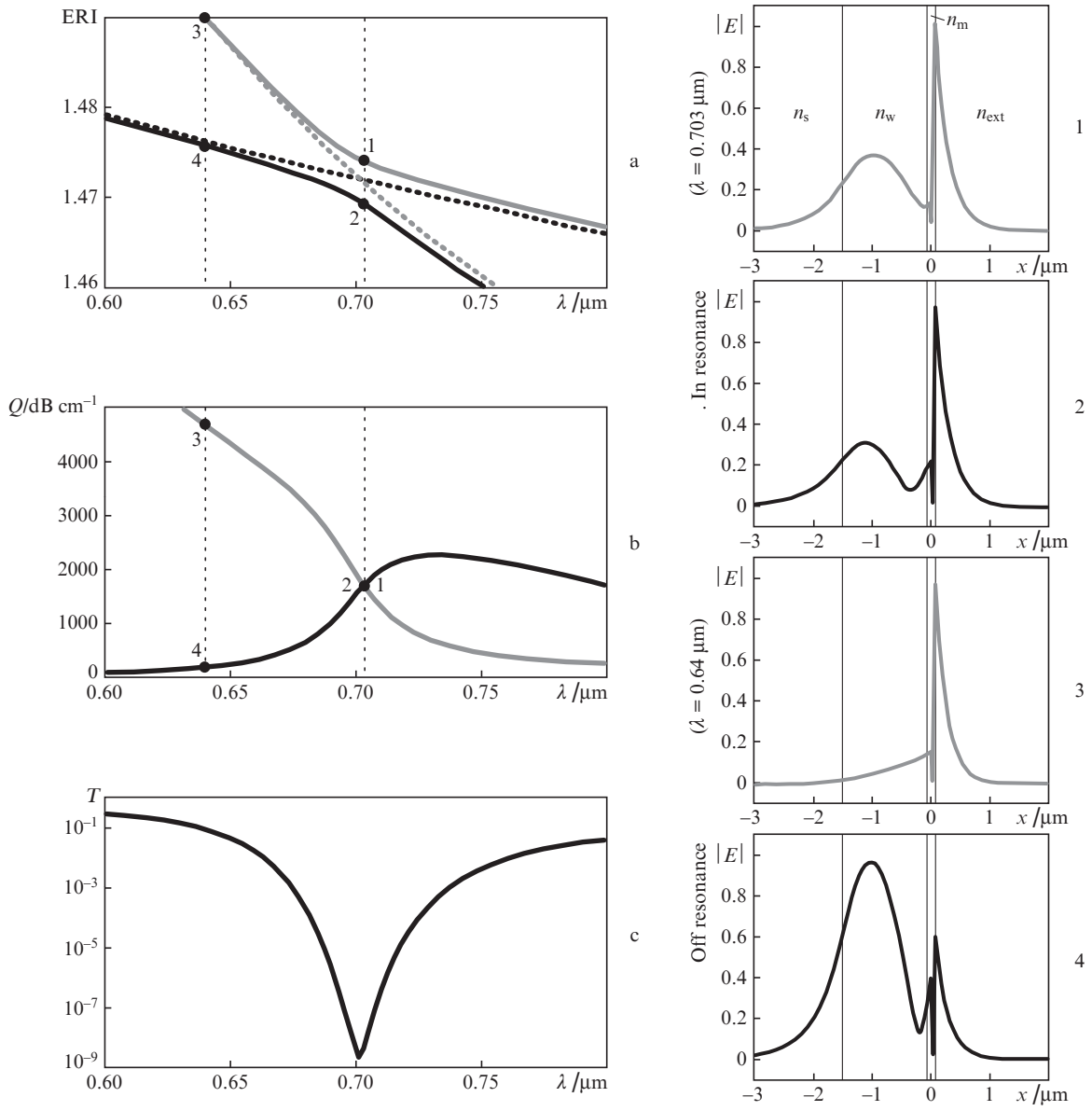

Figure 2. Spectral dependences of (a) the effective refractive index and (b) losses of the hybrid modes of the metallised segment, as well as (c) the transmission spectrum of the refractometer at $h_m = 60$ nm, $n_{ext} = 1.4$, $L = 500$ μm. Shown on the right are the MMS profiles at the resonance wavelength ($\lambda = 0.703$ μm, insets 1, 2) and the nonresonance one ($\lambda = 0.64$ μm, insets 3, 4).

guide mode, we mean the fundamental mode of the waveguide layer with the half-infinite substrate on one side and the half-infinite external medium on the other side.

According to the coupled mode theory, near the wavelength where WM and surface plasmon mode dispersion curves intersect, a considerable loss of guided radiation due to its energy transfer to the plasmon mode can occur in segment 2, provided that the coupling coefficient is sufficiently high. In particular, such losses arise for the metallic film thickness $h_m = 60$ nm, which is confirmed by the calculated ERI spectrum (Fig. 2a, solid curves), loss spectrum Q (Fig. 2b), and profiles (Fig. 2, insets 1–4) of hybrid modes of the multilayer structure (MMS) that forms segment 2 (see Fig. 1). As seen from insets 1 and 2 in Fig. 2, near the resonance wavelength the profiles of both MMS's comprise the elements of the waveguide mode and the plasmon one, i.e., represent a true result of their hybridisation. Since the MMS profiles are close to each other, they have similar overlap integrals with the profile of the fundamental mode in segment 1 and, therefore, are excited by it with nearly similar amplitudes. Their losses at this wavelength are equally high (~ 1700 dB cm^{-1}) and lead to the attenuation of the guided radiation power by nearly 80 dB, the length of the metallised segment being $L = 0.5$ mm. As seen from Fig. 2b and insets 3 and 4, aside the resonance the losses and the profiles of MMS strongly differ, and only the mode with low losses possesses an expressed maximum in the region of the waveguide layer and, therefore, is efficiently excited by the mode of segment 1. As a result, no essential attenuation of light occurs at this wavelength. Thus, an expressed dip arises in the transmission spectrum of the refractometer in the vicinity of the resonance wavelength (Fig. 2c).

The numerical calculations show that the resonance dip can be formed following two different scenarios, depending on the thickness of the metallic film. For the film thickness 68 nm and smaller, the anticrossing takes place in the spectral dependences of ERI of the hybrid MMS, while in the spec-

trum of losses the crossing is observed, which is illustrated by Figs 2a and 2b (h_m = 60 nm) and Figs 3a, 3b, 3e and 3f (h_m = 45 and 68 nm). For the film thickness 69 nm and greater, on the contrary, in the spectra of ERI the crossing is observed, whereas the loss spectra do not cross (Figs 3, 3i, 3j, 3m, 3n; h_m = 69, 74 nm).

These scenarios can be associated with two different regimes of coupling between the WM and the surface plasmon mode, considered separately. The first scenario can be considered as that corresponding to the strong coupling regime, in which a periodic exchange of energy occurs between the coupled modes at the resonance wavelength. This is illustrated by the distribution of the electric field amplitude of the guided radiation in segment 2 for the film thickness 45 nm, presented in Fig. 3d. From the point of view of the entire multilayer structure of segment 2, such an exchange corresponds to the interference beats of the hybrid MMS with the period $\lambda/\Delta n$, where Δn is the difference of their ERI at the resonance wavelength. Note that the period of the beats increases with increasing film thickness and, e.g., at h_m = 68 nm becomes greater than the characteristic length of the guided radiation damping. In this case the power exchange between the WM and surface polariton mode occurs so slowly that it is practically undistinguished against the background of the total light damping in segment 2 (Fig. 3h; h_m = 68 nm).

The second scenario of hybridisation can be associated with the regime of weak coupling, in which at the resonance wavelength there is no periodic power exchange between the waveguide and plasmon modes. From the point of view of the MMS, this corresponds to the situation when the interference beats between them do not arise due to the equality of propagation constants.

We emphasise that the terms 'strong coupling' and 'weak coupling' in the context of the present paper are understood

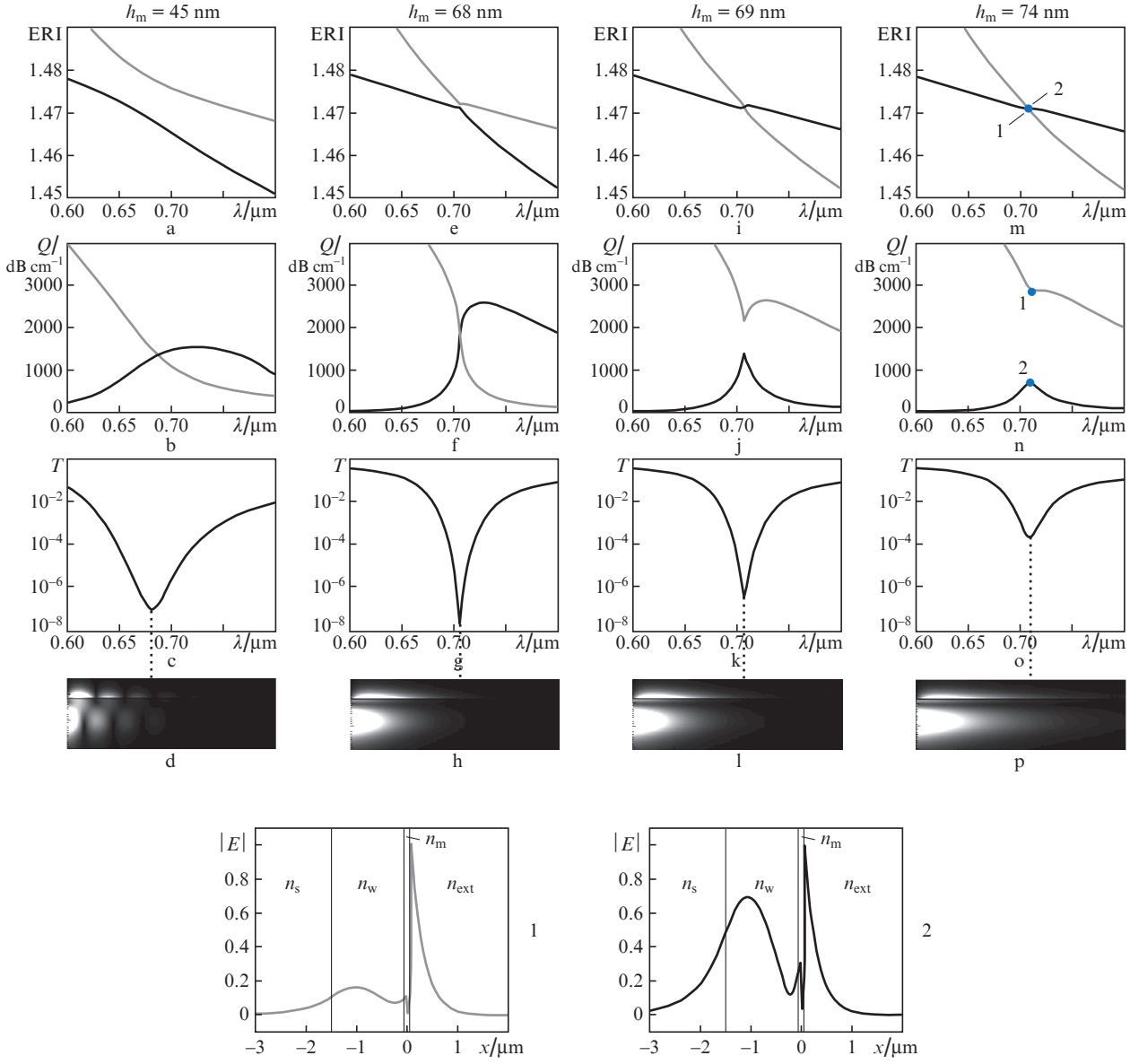

Figure 3. Dispersion curves of hybrid MMS, transmission spectra of the refractometer, and the amplitude distribution of the electric field of the guided radiation in the metallised segment at the resonance wavelength at n_{ext} = 1.4, L = 500 μm and h_m = (a, b, c, d) 45, (e, f, g, h) 68, (i, j, k, l) 69, and (m, n, o, p) 74 nm. In insets 1, 2 the profiles of MMS at the resonance wavelength at h_m = 74 nm are shown.

in a way different from that in the case of lossless mode coupling, and both terms refer to the resonance wavelength, at which the real parts of propagation constants of the coupled modes exactly coincide with each other.

From the coupled mode theory it follows [16] that the regime of coupling between the waveguide and plasmon modes is determined by the relation between the coupling coefficient D and the difference of their ERI, which at the resonance wavelength reduces to the imaginary part of the plasmon mode ERI n''_{SP} due to insignificant losses of WM. One can show that for $D > n''_{SP}$ the dependences of the coupled mode amplitudes on the coordinate directed along the waveguide are quasi-periodic, which corresponds to the regime of strong coupling, while for $D < n''_{SP}$ they acquire quasi-exponential character, corresponding to the regime of weak coupling.

The coupling coefficient between the waveguide and plasmon modes is firstly affected by the thickness of the metallic film: with an increase in h_m the profiles of the WM and the plasmon surface mode possess a smaller overlap, which leads to the reduction of D and, correspondingly, to weaker coupling. If the coupling becomes too weak ($D \ll n''_{SP}$), e. g., for $h_m = 74$ nm, the energy transfer from the waveguide mode to the plasmon wave becomes low-efficient, which significantly reduces the depth of the resonance dip (Fig. 3o). In terms of the MMS, this is explained by the fact that their profiles and losses at the resonance wavelength are different (see insets 1, 2 in Fig. 3), the profile shape of the MMS with smaller losses appearing closer to that of the mode in segment 1. As a result, it is stronger excited and stronger affects the resulting transmission of the entire structure, which leads to the observed reduction of the dip depth.

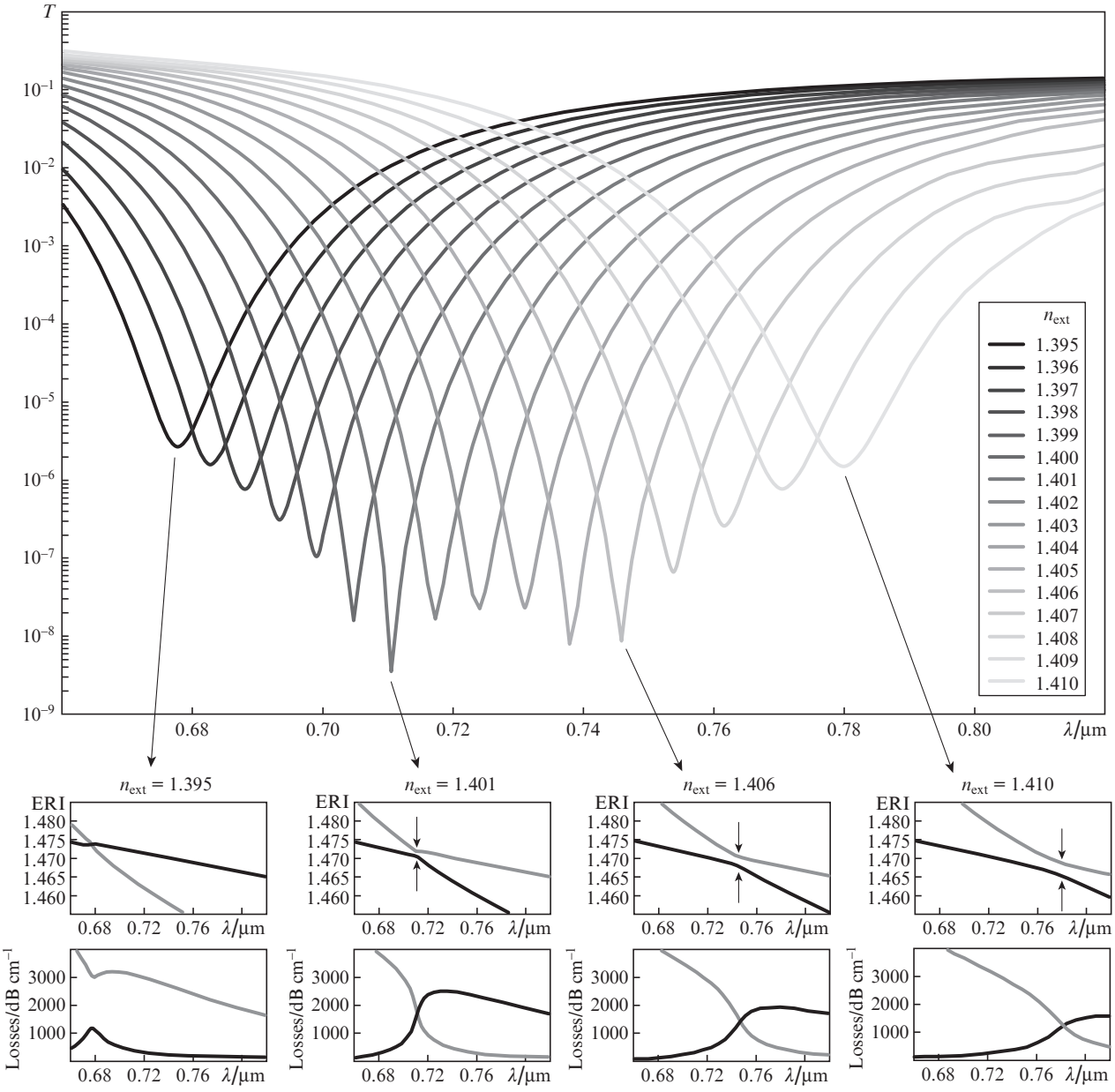

Figure 4. Calculated transmission spectra of the refractometer at $n_{ext} = 1.395–1.41$, $h_m = 68$ nm, and $L = 500$ μm. The insets present the dispersion dependences of the hybrid MMS at $n_{ext} = 1.395$, 1.401, 1.406, and 1.41.

On the other hand, if the coupling is too strong ($D \gg n''_{SP}$), e. g., at $h_m = 45$ nm, then the spectral range, in which it holds, essentially broadens, which leads to the broadening of the resonance dip (Fig. 3c). Thus, from the point of view of obtaining the maximal contrast of the dip, it is optimal to provide an intermediate situation near the transition between the regimes of strong and weak coupling. For $n_{ext} = 1.4$ it is implemented with the film thickness $h_m \approx 68$ nm (Fig. 3g).

However, the refractive index of the external medium does not remain constant in the process of refractometric measurements. Its variation leads to a shift of the resonance wavelength, which at the fixed value of h_m is inevitably accompanied by a change in the dip contrast. This is illustrated by Fig. 4 that shows the calculated transmission spectra of the refractometer, as well as the spectra of ERI and losses of the hybrid MMS at $h_m = 68$ nm, $n_{ext} = 1.395–1.41$, and $L = 0.5$ mm.

As seen from the MMS dispersion dependences presented in the insets of Fig. 4, as the resonance wavelength increases with increasing n_{ext}, the coupling between the WM and the surface plasmon mode becomes stronger. This is explained, first, by the broadening and more efficient overlapping of the waveguide and plasmon mode profiles, increasing the coupling coefficient. Second, the value of n''_{SP} that determines the losses of plasmon mode decreases with the growth of λ [6], which also enhances the coupling.

Thus, when λ_{SPR} increases with the growth of n_{ext}, the depth of the resonance dip at first gradually increases, as the coupling becomes stronger, but the weak coupling regime still takes place ($n_{ext} < 1.4$). At $n_{ext} \approx 1.4$ the switching to the strong coupling regime occurs with subsequent coupling enhancement as λ_{SPR} shifts with the growth of n_{ext}, as seen from the increasing difference of ERI of hybrid modes at the resonance wavelength (shown by arrows in Fig. 4 insets).

At $n_{ext} > 1.4$ one can also observe small quasi-periodic variations of the resonance dip depth. They are caused by a periodic power exchange between the waveguide mode and the plasmon one, due to which at the output of segment 2 the guided radiation depending on the exchange period appears to be mainly localised either in the waveguide layer, or near the metallic film, affecting the transition losses at the boundary between segments 2 and 3. The exchange period decreases as the coupling becomes stronger with the growth of λ_{SPR}, which leads to the observed variations of the dip depth due to the change of the above transition losses.

When the measured RI exceeds $n_{ext} = 1.406$, the width of the resonance dip increases, because the coupling between WM and the surface plasmon mode becomes too strong, and the depth decreases due to the reduction of surface plasmon mode losses with the wavelength growth.

Thus, the range of efficient measurement of the external medium RI (Δn_{ext}) can be conditionally defined as the region of n_{ext} values, for which the resonance dip depth is smaller than the maximal one by not greater than a certain threshold value, e. g., 20 dB. In the considered case, as seen from Fig. 4, this nearly corresponds to the range $n_{ext} = 1.395–1.41$, i. e., $\Delta n_{ext} \approx 0.015$. From the analysis of this Figure it also follows that the spectral sensitivity of the refractometer $S_{RI} \approx 6800$ nm (per unit of refractive index), and the logarithmic half-width of the resonance dip FWSRM in the middle of

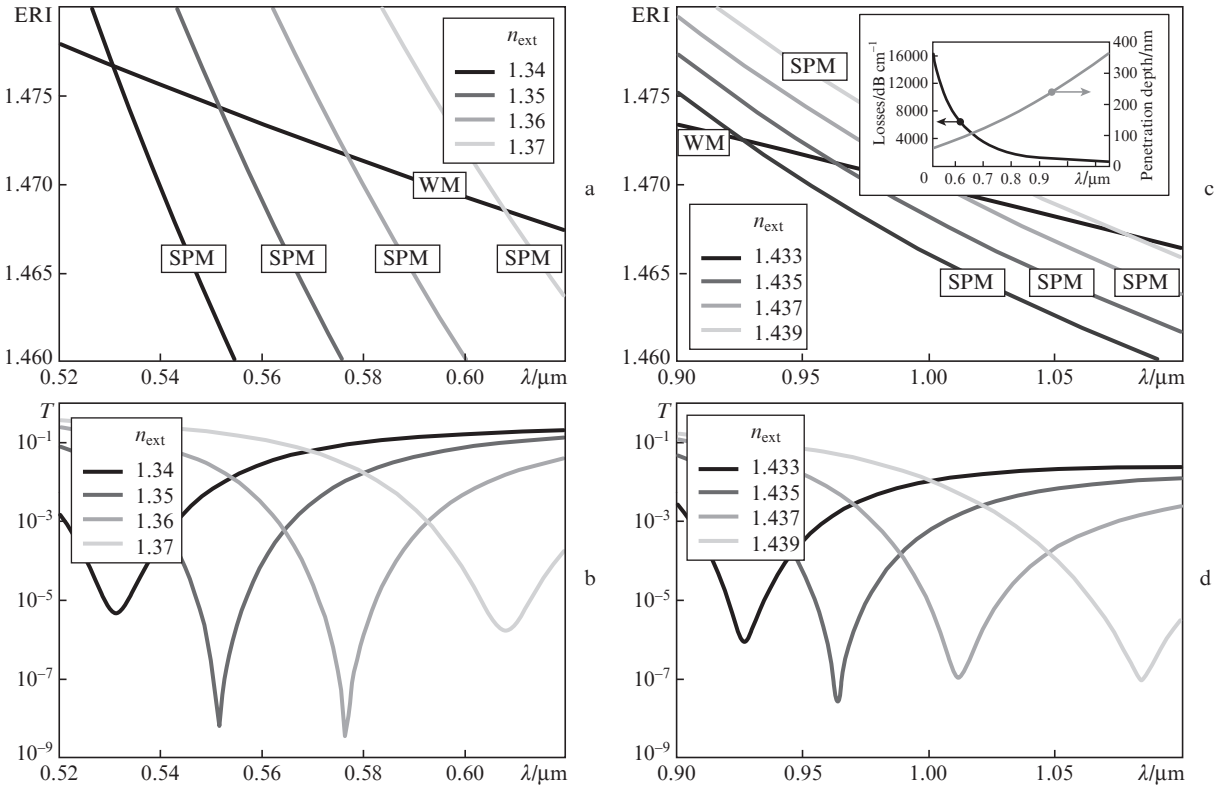

Figure 5. Spectral dependences of ERI for the waveguide and surface plasmon modes, considered separately, and transmission spectra of the refractometer for (a, b) $h_m = 58$ nm, $h_w = 1$ μm, $L = 0.2$ mm, $n_{ext} = 1.34–1.37$ and for (c, d) $h_m = 75$ nm, $h_w = 2.5$ μm, $L = 1.3$ mm, $n_{ext} = 1.433–1.439$. The inset shows the spectral dependence of losses and depth of the surface plasmon mode (SPM) penetration into the external medium.

the n_{ext} measurement range amounts to ~25 nm. The depth of plasmon mode penetration into the external medium d_{SP} near the wavelength λ = 700 nm amounts to ~120 nm (see the inset in Fig. 5), which yields FOM ≈ 270 and RLC ≈ 0.44.

Note that the considered configuration of the SPR refractometer can be used for measuring other values of the refractive index of the external medium, both greater and smaller than 1.4. For example, for $n_{ext} \approx 1.35$ the phase matching between the plasmon mode and the waveguide one can be provided near the wavelength λ = 550 nm (Fig. 5a). In this case, the optimal thickness of the silver film amounts to 58 nm. To maintain the single-mode operation of the waveguide layer at this wavelength, it is reasonable to reduce its thickness to 1 μm. Since the losses of the plasmon mode in this spectral range are by a few times higher than for $\lambda \approx 700$ nm (see inset in Fig. 5), the length of the sensitive segment is reduced to 0.2 mm.

In spite of higher losses for the surface plasmon mode, the width of the resonance dip in this case appears smaller than in the previous one: FWSRM ≈ 16 nm (for n_{ext} = 1.35), which is explained by essentially greater intersection angle of dispersion curves for the waveguide and plasmon modes (see Fig. 5a). For the same reason, although the physical sensitivity of plasmon mode to the RI of the external medium grows with decreasing wavelength [6], S_{RI} appears in this case to be nearly by two and a half times lower than at $\lambda \approx 700$ nm because of the strong reduction of the instrumental contribution ($S_{RI} \approx 2600$ nm). The range of refractometric measurements in this case increases to $\Delta n_{ext} \approx 0.03$. Thus, FOM ≈ 162, which is by more than one and a half times smaller than in the previous case. However, the depth of plasmon mode penetration into the external medium at $\lambda \sim 550$ nm amounts to only ~70 nm (see inset in Fig. 5), so that from the point of view of measuring local variations of RI in a thin layer there is practically no difference from the previous case: RLC ≈ 0.43.

For higher values of the refractive index of the external medium ($n_{ext} \approx 1.435$), the phase matching between the waveguide and plasmon modes can be provided near the wavelength λ = 1000 nm (Fig. 5c). The optimal film thickness in this case amounts to 75 nm and the thickness of the waveguide layer is 2.5 μm.

The specific features of this range are, first, the lower losses of the surface plasmon mode than at $\lambda \sim 700$ nm and $\lambda \sim 550$ nm, so that to obtain the dip depth of ~80 dB one has to increase the sensitive segment length to 1.3 mm. Second, the dispersion curves for the WM and surface plasmon mode cross at much smaller angle than in both previous cases. This leads to a considerable increase in the spectral sensitivity due to an increase in the instrumental contribution ($S_{RI} \approx 26000$ nm), the reduction of the refractometric measurement range ($\Delta n_{ext} \approx 0.008$) and the resonance dip broadening. The latter feature is partially compensated for by lower losses of the surface plasmon mode, which finally yields FWSRM ≈ 44 nm. Thus, by the combination of the sensitivity and the dip width in this case we have a considerable advantage: FOM ≈ 590. However, from the point of view of measuring local variations of RI in a thin layer, there is practically no difference from the previous two cases: RLC ≈ 0.46 at the expense of large penetration depth of the plasmon mode field into the external medium at $\lambda \sim 1000$ nm ($d_{SP} \approx 270$ nm).

3.2. SPR refractometer based on the symmetric plasmon mode

The introduction of a buffer layer between the waveguide and the metallic film (see Fig. 1b) with the refractive index close to that of the external medium provides the possibility of constructing an SPR refractometer using the excitation of both symmetric and antisymmetric plasmon modes [6]. The SPM and ASPM essentially differ in their properties both from each other and from the above surface plasmon mode. Therefore, the metrological characteristics of the SPR refractometer with a buffer layer may essentially differ from the characteristics of the refractometer without a buffer layer. To improve the measurement parameters, one has to exploit more efficiently the advantages of each plasmon mode in the SPR refractometer design.

In particular, the main advantage of the symmetric plasmon mode is its low level of losses [6, 10–12]. This fact allows one to obtain a relatively narrow resonance dip even at the smallest intersection angle of the WM and SPM dispersion curves, thus providing an extremely high spectral sensitivity at the expense of large instrumental contribution. The SPM losses decrease with increasing wavelength and decreasing film thickness [6], so that for the SPR refractometer construction it is reasonable to use thin films and long-wavelength spectral range. However, the film being too thin does not satisfy technological and practical requirements, and at too large λ_{SPR} the crossing angle of the WM and SPM dispersion curves can become too small for obtaining a high-contrast resonance dip, notwithstanding the low SPM losses. Therefore, as a trade-off version, we choose h_m = 20 nm and the operating wavelength near λ = 1000 nm.

Note also that the symmetric plasmon mode has a considerably smaller effective refractive index than the surface plasmon mode and the ASPM, so that to provide its phase matching with the waveguide mode one has to use materials with a low optical density. The above conditions are satisfied if, e.g., the structure is such: the substrate of Cytop polymer ($n_s \sim 1.34$ [18]), the waveguide layer of MgF_2 ($n_w \sim 1.37$ [19], h_w = 200 nm), the buffer layer of Cytop ($n_b \sim 1.34$ [19]), and the film of silver (h_m = 20 nm).

Figure 6a presents the calculated dispersion dependences of separately considered WM and SPM at n_{ext} = 1.33. It is seen that the phase matching condition between them at the given value of the external medium RI is satisfied near λ = 1040 nm. To provide the maximal dip contrast in the refractometer transmission spectrum, the switching of the WM–SPM coupling regime should also occur near this wavelength. In the present configuration, in contrast to the SPR refractometer without a buffer layer, the regime of coupling between the WM and SPM is affected, firstly, by the thickness of the buffer layer h_b. The calculations show that the optimal value of h_b, for which the coupling regime transition occurs at $n_{ext} \sim 1.33$ near λ = 1040 nm amounts to 13.3 μm (Figs 6b, 6c, 6e, and 6f).

The calculated transmission spectra of the refractometer for n_{ext} = 1.3299–1.3302, h_b = 13.3 μm are presented in Fig. 6d. The spectral sensitivity S_{RI} in this case amounts to ~120000 nm, the measurement range is $\Delta n_{ext} \approx 0.0004$, the half-width of the resonance dip FWSRM ≈ 18 nm (for $n_{ext} \sim 1.3301$), i.e., FOM ≈ 6670, which exceeds the analogous parameter of the SPR refractometer without a buffer layer by more than an order of magnitude. Although the depth of

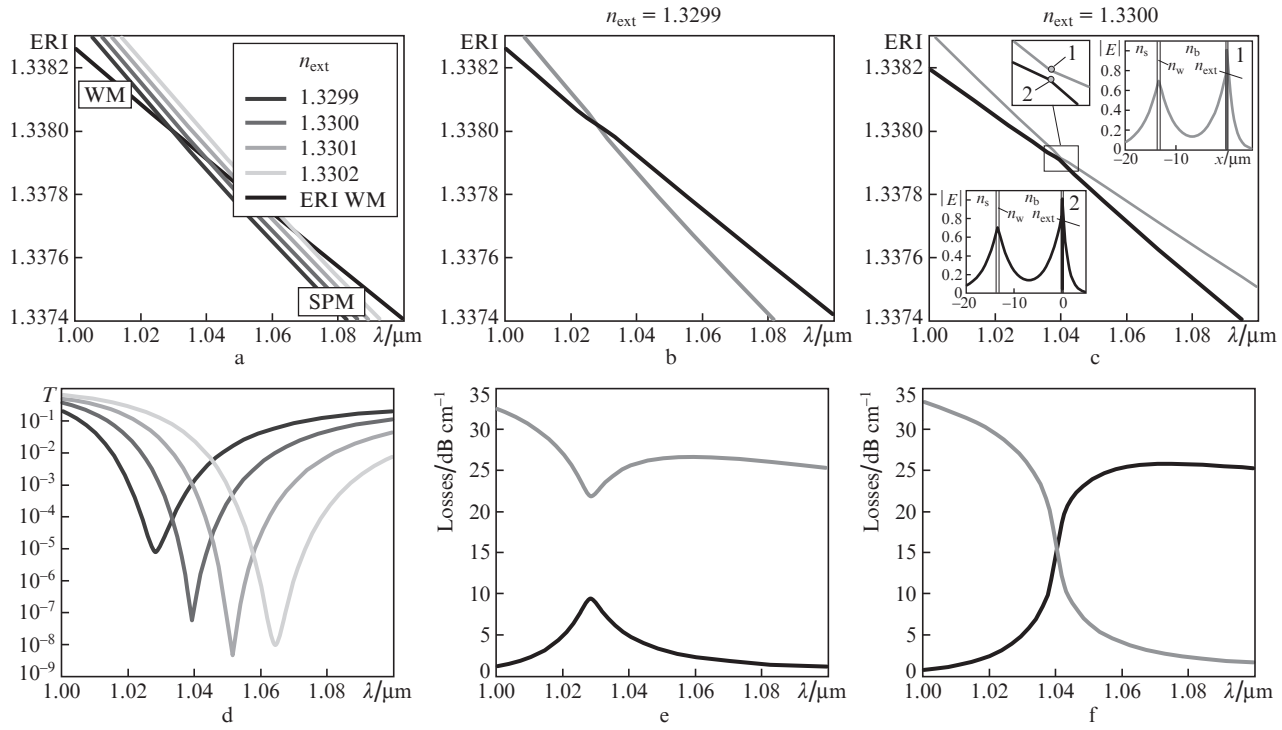

Figure 6. (a) Dispersion dependences of waveguide and symmetric plasmon modes considered separately and (d) the refractometer transmission spectra for n_{ext} = 1.3299–1.3302; the spectral dependences of ERI and the losses of hybrid MMS of the metallised segment for n_{ext} = (b, e) 1.3299 and (c, f) 1.33 (L = 60 mm, h_w = 200 nm, h_b = 13.3 μm, h_m = 20 nm). The inset in Fig. 6c shows the profiles of hybrid MMS at the resonance wavelength at n_{ext} = 1.33.

SMP penetration into the external medium is much greater than that for the surface plasmon mode and amounts to ~580 nm for $\lambda \sim 1050$ nm, from the point of view of local resolution we also have a considerable advantage: RLC ≈ 0.09, which is nearly by five times lower than the RLC of the refractometer without a buffer layer. Note that the achieved advantage in metrological characteristics is provided due to the low losses of SPM (~30 dB cm^{-1} for $\lambda \sim 1050$ nm). Therefore, it is inevitably associated with the increase in the sensitive segment length (the resonance dip depth of ~80 dB is provided in this case at L = 6 cm).

If necessary, the length of the sensitive element can be decreased, choosing the structure parameters such that the plasmon resonance condition would be satisfied in shorter-wavelength spectral range, where the SPM has higher losses. For example, for the waveguide layer thickness h_w = 400 nm the plasmon resonance for $n_{ext} \sim 1.33$ arises near the wavelength λ = 600 nm. The optimal thickness of the buffer layer in this case amounts to 2.6 μm. The losses of the symmetric plasmon mode at this wavelength appear to be by nearly an order of magnitude higher than at $\lambda \sim 1000$ nm and amount to 310 dB cm^{-1}, which allows the reduction of the sensitive segment length by 10 times: L = 6 mm. The spectral sensitivity also appears smaller almost by an order of magnitude because of the strong reduction of the instrumental contribution ($S_{RI} \approx 16000$ nm), which is accompanied by an increase in the measurement range ($\Delta n_{ext} \approx 0.003$) and a certain narrowing of the resonance dip (FWSRM ≈ 12 nm). Thus, with the sensitivity and dip width as a whole, this SPM refractometer configuration is inferior to the previous one by five times (FOM ≈ 1330). However, due to the smaller depth of SPM penetration into the external medium at $\lambda \sim 600$ nm ($d_{SP} \approx 200$ nm), the local resolution of the refractometer is insignificantly worse: RLC ≈ 0.15.

3.3. SPR refractometer based on the antisymmetric plasmon mode

From the analysis of properties of the antisymmetric plasmon mode [6, 13, 14] one can conclude that from the point of view of constructing a SPR refractometer the ASPM advantage is, first, the higher degree of the field localisation, which potentially provides a higher local sensitivity to the variations of the refractive index n_{ext} in a thin layer. Second, it possesses a higher physical sensitivity to the variation of the refractive index n_{ext} in comparison with SPM. Third, the high losses of ASPM allow one to obtain a deep resonance dip using the minimal length of the sensitive element. All these specific features become more expressed with a decrease in the metallic film thickness and the wavelength [6]. Besides that, as shown by calculations, at different refractive indices of the media, located on different sides of the film, the ASPM profile is shifted towards the optically denser medium, which additionally increases the physical sensitivity to the medium RI.

Thus, for the most complete realisation of the ASPM advantages in the SPR refractometer construction, it is reasonable to use, first, a short-wavelength spectral range, second, a sufficiently thin metallic film, and, third, the RI of the buffer layer smaller than that of the external medium. Besides that, keeping in mind that the ERI of the antisymmetric plasmon mode is rather high [6], for its phase matching with the WM the material of the waveguide layer should possess a sufficiently high optical density. The above conditions are satisfied, e. g., for the following structure: the substrate of SiO_2, the waveguide of Si_3N_4 ($n_w \sim 2$ [20], h_w = 250 nm), the buffer layer of Teflon AF2400 ($n_b \sim 1.28$ [21]), the film of silver (h_m = 20 nm), and the external medium ($n_{ext} > n_b$).

Figure 7a presents the dispersion dependences of separately considered waveguide and antisymmetric plasmon modes

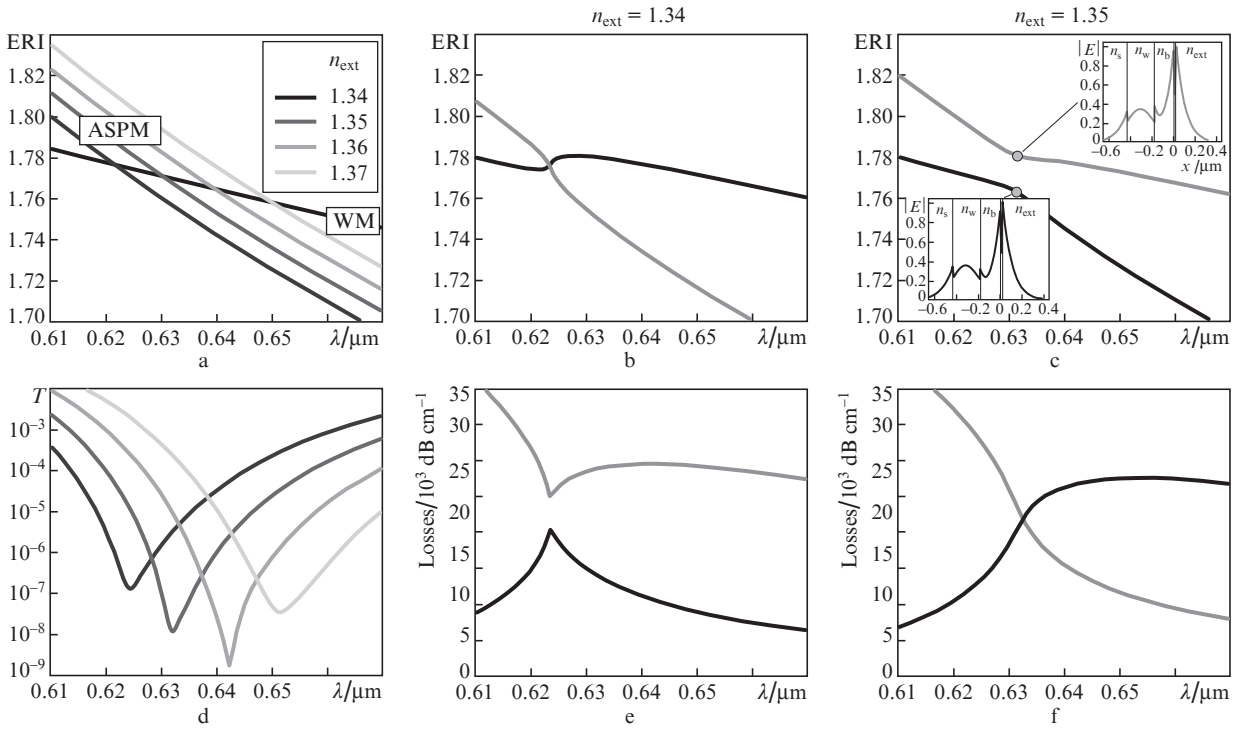

Figure 7. (a) Dispersion dependence of the separately considered waveguide and antisymmetric plasmon modes and (d) the transmission spectra of the refractometer at n_{ext} = 1.34–1.37; the spectral dependences of ERI and the losses of hybrid MMS of the metallised segment for n_{ext} = (b, e) 1.37 and (c, f) 1.35 (L = 0.04 mm, h_w = 250 nm, h_b = 180 nm, h_m = 20 nm). The insets in Fig. 7c show the profiles of the hybrid MMS at the resonance wavelength for n_{ext} = 1.35.

at different values of n_{ext} in the range 1.34–1.37. As seen from the figure, the phase matching between them under the chosen parameters of the waveguide structure can be provided at $\lambda \sim 640$ nm, where, as shown by calculations, the ASPM losses amount to ~42000 dB cm^{-1}. The optimal thickness of the buffer layer h_b, for which near this wavelength the switching of the WM–ASPM coupling regime occurs, amounts to 180 nm (Figs 7b, 7c, 7e, and 7f). The losses of hybrid MMS at the resonance wavelength in this case approach ~22000 dB cm^{-1}, which allows the reduction of the sensitive segment length to 40 μm.

The calculated transmission spectra of the refractometer at n_{ext} = 1.34–1.37 are presented in Fig. 7d. As follows from the figure, the spectral sensitivity of the refractometer is $S_{RI} \approx$ 900 nm, the range of measurement is $\Delta n_{ext} \approx 0.03$, the dip half-width is ~35 nm (for n_{ext} = 1.36), which yields FOM ≈ 25.7. This is nearly by an order of magnitude lower than in the case of the SPR refractometer without a buffer layer and by 260 times lower than in the SPR refractometer using SPM. The depth of penetration of ASPM into the external medium in the vicinity of the wavelength λ = 640 nm amounts to only 44 nm, and, therefore, RLC ≈ 1.7.

Note that such a low spectral sensitivity is caused by the small instrumental contribution due to the large intersection angle of the WM and ASPM dispersion curves. By adjusting the structure parameters so that the plasmon resonance would arise in a longer wavelength region, one can reduce the intersection angle of dispersion curves and, therefore, obtain a higher spectral sensitivity. The dip width in this case also increases, but due to the ASPM losses reduction with the wavelength growth a certain cumulative advantage in spectral sensitivity and dip width can be obtained, which, however is achieved at the expense of the compactness of the measuring transducer.

For example, with a waveguide layer thickness of 150 nm the condition of plasmon resonance is fulfilled for $n_{ext} \sim 1.33$ near the wavelength λ = 900 nm, where the losses of ASPM amount to ~11000 dB cm^{-1}. At the optimal thickness of the buffer layer (h_b = 568 nm) the resonance dip ~80 dB deep is achieved at a length of the sensitive segment L = 180 μm. The spectral sensitivity in this case amounts to 3700 nm, the measurement range $\Delta n_{ext} \approx 0.02$, the dip half-width WSRM ≈ 65 nm, the depth of plasmon wave penetration into the external medium $d_{SP} \approx$ 117 nm, which yields FOM ≈ 57 and RLC ≈ 2.05.

4. Discussion of results

The metrological characteristics of the three studied configurations of a SPR refractometer are summarised in Table 1.

One can see that the main cause of difference in metrological characteristics of the studied refractometers is the different spectral sensitivity. The physical sensitivity changes insignificantly, and the observed differences are mainly caused by the different instrumental contributions.

The best metrological characteristics are inherent in the SPR refractometer using SPM: due to the small losses, a high-contrast resonance dip is attainable at a very small intersection angle of the WM and SPM dispersion curves, which provides an extremely high instrumental sensitivity. The advantage in the FOM parameter, characterising the spectral sensitivity and the dip width cumulatively, attains nearly two orders of magnitude as compared to the SPR refractometer based on

ASPM and an order of magnitude compared to the SPR refractometer without a buffer layer.

In addition to low losses, SPM is characterised also by the depth of penetration into the external medium greater than that of ASPM and the surface plasmon mode. Therefore, from the point of view of measuring the local RI variations in a thin layer, the advantage of using SPM is less expressed – for the coefficient of local resolution the advantage amounts to ~ 20 as compared to the SPR refractometer using ASPM and ~ 5 compared to SPR refractometer without the buffer layer.

It is worth noting that the metrological advantages of the SPR refractometer based on SPM are achieved at the expense of compactness of the measuring transducer: to obtain the similar depth of the resonance dip as in the refractometers based on ASPM and surface plasmon modes one has to use significantly longer (up to three orders of magnitude) sensitive segments.

The minimal length of the sensitive segment and, therefore, the maximal compactness of the measuring transducer are achieved in the SPR refractometer based on the ASPM, which, however, possesses the worst metrological characteristics due to extremely high losses of ASPM.

The SPR refractometer without a buffer layer occupies the intermediate position between the refractometers based on SPM and ASPM both in metrological characteristics and the length of the sensitive segment. However, it favourably differs from them by the simplicity of optical scheme and, correspondingly, the simplicity of fabrication, which is an important advantage from the practical point of view.

From Table 1 one can see that the measured value of the refractive index depends on the parameters of the metallised segment and the operating spectral range. Choosing a longer-wavelength range, where the plasmon mode has smaller losses and, hence, increasing the length of metallised segment, one can acquire a cumulative advantage in sensitivity and dip width. However, the local resolution coefficient in this case changes insignificantly, because the increased depth of plasmon mode penetration into the external medium compensates the growth of FOM. Note also that in the case of an excessive shift of the resonance wavelength towards the infrared region ($\lambda_{SPR} > 1200$ nm) the intersection angle of dispersion curves of the waveguide and plasmon modes can be so small and the width of the dip so large that the refractometric measurements will become inefficient in spite of very high sensitivity.

Note in conclusion that the values of the measured refractive index of the external medium presented in Table 1 and the corresponding wavelengths are determined by the particular choice of materials and parameters of the metallised segment and, therefore, can vary. However, the revealed trends and regularities remain valid.

5. Conclusions

Thus, we have studied three configurations of a SPR refractometer: the one having no buffer layer and using the surface plasmon mode and the ones having a buffer layer and using the excitation of symmetric and antisymmetric plasmon modes.

It is shown that in order to provide the highest metrological characteristics of the refractometer it is reasonable to use SPM; however, it is related to a considerable increase in the sensitive element length.

In the case when the main requirement to the refractometer is its minimal size, the optimal way is to use the ASPM, which allows minimisation of the sensitive segment length at the expense of metrological characteristics.

Finally, from the point of view of fabrication simplicity the most attractive configuration is the SPR refractometer without a buffer layer, which occupies an intermediate position between the refractometers based on ASPM and SPM both in metrological characteristics and in length of the sensitive segment.

Acknowledgements. The work was supported by the Russian Scientific Foundation (Grant No. 16-12-10165).

Table 1.

Parameter	SPR refractometer						
	Without a buffer layer			With a buffer layer using SPM		With a buffer layer using ASPM	
Measured RI	1.355 ± 0.015	1.404 ± 0.0075	1.437 ± 0.004	1.33 ± 0.0015	1.3301 ± 0.0002	1.355 ± 0.015	1.33 ± 0.01
Operating spectral range /nm	530–610	680–780	920–1120	600–650	1030–1080	625–655	900–980
Instrumental sensitivity, S_1	2000	6000	24000	34000	316000	825	4350
Physical sensitivity, S_2	1.26	1.14	1.08	0.47	0.38	1.09	0.85
Spectral sensitivity $S_{RI} = S_1 S_2$ /nm	2600	6800	26000	16000	120000	900	3700
Dip half-width FWSRM /nm	16	25	44	12	18	35	65
FOM	162	270	590	1330	6670	25.7	57
Plasmon mode losses near λ_{SPR} /dB cm^{-1}	11620	3650	970	310	30	42000	11000
Length L (in mm) at the dip depth ~ 80 dB	0.2	0.5	1.3	6	60	0.04	0.18
Penetration depth d_{SP} /nm	70	120	270	200	580	44	117
CLR	0.43	0.44	0.46	0.15	0.09	1.7	2.05

References

1. Rasooly A., Herold K.E. (Eds). *Biosensors and Biodetection* (Totowa, NJ: Humana Press, 2009).
2. Guo X. *J. Biophoton.*, **5**, 483 (2012).
3. Baldini F. et al. *Optical Chemical Sensors* (Erice, Italy: Springer Science & Business Media, 2006) Vol. 224.
4. Ligler F.S., Taitt C.R. (Eds). *Optical Biosensors: Today and Tomorrow* (Oxford: Elsevier, 2011).
5. Homola J. *Chem. Rev.*, **108** (2), 462 (2008).
6. Homola J. *Surface Plasmon Resonance Based Sensors, Springer Series on Chemical Sensors and Biosensors* (Berlin – Heidelberg: Springer-Verlag, 2006).
7. https://www.hindawi.com/journals/js/2009/979761/cta/.
8. Caucheteur C., Guo T., Albert J. *Analytical and Bioanalytical Chemistry*, **407** (14), 3883 (2015).
9. Klantsataya E. et al. *J. Sensors*, **17** (1), 12 (2016).
10. Nenninger G.G. et al. *Sensors and Actuators B: Chem.*, **74** (1 – 3), 145 (2001).
11. Slavík R., Homola J. *Sensors and Actuators B: Chem.*, **123** (1), 10 (2007).
12. Jakub D., Kasry A., Knoll W. *Plasmonics*, **2** (3), 97 (2007).
13. Fan B., Liu F., Li Y., Huang Y., Miura Y., Ohnishi D. *Appl. Phys. Lett.*, **100** (11), 111108 (2012).
14. Fan Boyu et al. *Sensors and Actuators B: Chem.*, **186**, 495 (2013).
15. Palik E.D. *Handbook of Optical Constants of Solids* (San Diego: Acad. Press, 1998).
16. Snyder A.W., Love J. *Optical Waveguide Theory* (Erice, Italy: Springer Science & Business Media, 2012).
17. Sultanova N., Kasarova S., Nikolov I. *Acta Phys. Polonica-Ser. A General Phys.*, **116** (4), 585 (2009).
18. http://www.bellexinternational.com/products/cytop/pdf/cytop-catalog.pdf.
19. Li H.H. *J. Phys. Chem. Ref. Data*, **9** (1), 161 (1980).
20. Philipp H.R. *J. Electrochem. Soc.*, **120** (2), 295 (1973).
21. Yang Min K., French R.H., Tokarsky E.W. *J. Micro/ Nanolithography, MEMS and MOEMS*, **7** (3), 033010 (2008).